

## A catalogue of 323 cataclysmic variables from LAMOST DR6

YONGKANG SUN<sup>a,1</sup>, ZHENGHAO CHENG<sup>a,1</sup>, SHUO YE,<sup>2</sup> RUOBIN DING,<sup>1</sup> YIJIANG PENG,<sup>1</sup> JIAWEN ZHANG,<sup>1</sup> ZHENYAN HUO,<sup>1</sup>  
WENYUAN CUI,<sup>1</sup> XIAOFENG WANG,<sup>3,4</sup> JIANRONG SHI,<sup>5,6</sup> JIE LIN,<sup>3</sup> CHENGYUAN WU,<sup>3</sup> LINLIN LI,<sup>1</sup> SHUAI FENG,<sup>1</sup> YANG YU,<sup>1</sup>  
XIAORAN MA,<sup>3</sup> XIN LI,<sup>4</sup> CHENG LIU,<sup>4</sup> ZIPING ZHANG,<sup>4</sup> AND ZHENZHEN SHAO<sup>4</sup>

<sup>1</sup>College of Physics, Hebei Normal University, Shijiazhuang 050024, China

<sup>2</sup>Software College, Hebei Normal University, Shijiazhuang 050024, China

<sup>3</sup>Physics Department, Tsinghua University, Beijing 100084, China

<sup>4</sup>Beijing Planetarium, Beijing Academy of Sciences and Technology, Beijing 100044, China

<sup>5</sup>School of Astronomy and Space Science, University of Chinese Academy of Sciences, Beijing 100049, China

<sup>6</sup>Key Laboratory of Optical Astronomy, National Astronomical Observatories, Chinese Academy of Sciences, Beijing 100012, China

Submitted to ApJS

### ABSTRACT

In this work, we present a catalogue of cataclysmic variables (CVs) identified from the Sixth Data Release (DR6) of the Large Sky Area Multi-Object Fiber Spectroscopic Telescope (LAMOST). To single out the CV spectra, we introduce a novel machine-learning algorithm called UMAP to screen out a total of 169,509 H $\alpha$ -emission spectra, and obtain a classification accuracy of the algorithm of over 99.6% from the cross-validation set. We then apply the template matching program PyHammer v2.0 to the LAMOST spectra to obtain the optimal spectral type with metallicity, which help us identify the chromospherically active stars and potential binary stars from the 169,509 spectra. After visually inspecting all the spectra, we identify 323 CV candidates from the LAMOST database, among them 52 objects are new. We further discuss the new CV candidates in subtypes based on their spectral features, including five DN subtype during outbursts, five NL subtype and four magnetic CVs (three AM Her type and one IP type). We also find two CVs that have been previously identified by photometry, and confirm their previous classification by the LAMOST spectra.

*Keywords:* cataclysmic variable stars, catalogues, spectral classification

### 1. INTRODUCTION

Cataclysmic variable stars (CVs) are semi-detached binary systems with short orbital periods ranging from shorter than one hour to longer than six hours (Warner 2003; Zorotovic et al. 2016). They typically consist of a white dwarf star and a late-type main-sequence companion. With the loss of angular momentum, the mass transfer is continuously or intermittently activated through the inner Lagrangian point of the Roche lobe, usually leading to the formation of an accretion disc.

The CVs can be divided into several types: classical nova (CN), recurrent nova (RN), dwarf nova (DN), nova-like variables (NL), polars (or AM Her type), and inter-

mediate polars (IPs, including DQ Her type) (Warner 2003). The latter two are magnetic CVs. Note that in polars, the magnetic field is typically stronger than 20 MG that an accretion disc can not form. Classical novae usually have only one observed eruption by definition. If a classical nova is observed with a second eruption, it will be classified as a recurrent nova. Dwarf novae usually have frequent and regular bursts as a result of instability of the accretion disk (Morales-Rueda & Marsh 2002). U Gem stars are the prototype of DN subtype of CVs which have repeated normal outbursts. The SU UMa subtype of DNs presents superhumps in addition to normal outbursts and the Z Cam subtype of DNs are characteristic of standstills in the light curve (Szkody 1987; Hellier 2001). Nova-like objects (NLs) are recognized as novae between eruptions and do not have a recorded outburst. Some NLs have been observed to occasionally change from a high state with higher bright-

ness to a low state with lower brightness (La Dous 1994; King & Cannizzo 1998; Rodríguez-Gil et al. 2015). In the AM Her systems, the magnetic field of the white dwarf is strong enough for both stars to be locked into the same rotation period. In this system, the mass flow is controlled by the magnetic field and falls directly toward the surface of the white dwarf. Correspondingly, the accretion disk of IPs is truncated at the radius of the magnetosphere. Sometimes these two types of magnetic CVs are referred to jointly as one subtype of nova-like variables (Coppejans et al. 2015).

As a special kind of interacting binary systems, CVs have complex physical processes and unique observation properties in various wave bands and show luminosity variations of different time scales and amplitudes. They are important samples that help us to understand the evolution of binary stars and even the explosion mechanism of type Ia supernovae (SNe Ia) (Hachisu & Kato 2001; Anupama 2011). The acquisition and analysis of more CV samples are helpful to the refining of the theoretical models of CVs.

So far, numerous works have been conducted to search for CVs. Downes et al. (2001) published a catalogue including spectra, which is a revision and supplement to the first two editions (Edition 1 - Downes & Shara (1993) and Edition 2 - Downes et al. (1997)). This catalogue consists of 1034 CVs and 194 non-CV objects. Using the Sloan Digital Sky Survey (SDSS) I/II, Szkody et al. (2011) published a summary table of 285 CVs with the SDSS spectra. Jiang et al. (2013) identified CVs from the low-resolution spectra of LAMOST by using the support vector machine technique (SVM) combined with principal component analysis (PCA). They identified 10 cataclysmic variables, of which two are new CV candidates. Breedt et al. (2014) provided spectroscopic identification of 85 systems fainter than  $g \geq 19$  mag and analyzed the photometric properties of the 1043 CV candidates from the Catalina Real-time Transient Survey (CRTS). Coppejans et al. (2016) published an outburst catalogue which contains a wide variety of observational properties for 722 dwarf nova-type CVs and 309 CVs of other types from the CRTS. By cross-matching the published catalogues with LAMOST DR3, Han et al. (2018) collected 48 known CVs, and they found three new CVs using the method adopted by Jiang et al. (2013). Szkody et al. (2020) published 329 objects as known or candidate CVs during the first year of testing and operation of the Zwicky Transient Facility. Hou et al. (2020) used the Bagging and the Random Forest algorithms to search for CVs from LAMOST DR5, and they identified 245 cataclysmic variables, of which 52 CV candidates are new.

In this work, we present a catalogue of 323 CV candidates identified from LAMOST DR6, of which 52 objects are new. The structure of this paper is as follows. Section 2 describes the method and process to identify the CV candidates according to the spectral features. Section 3 presents the results. Section 4 is the discussion of the spectral properties and subtype classification of the LAMOST CV candidates. Section 5 is the summary.

## 2. DATA

The Large Sky Area Multi-Object Fiber Spectroscopic Telescope (LAMOST) is a 4-meter quasi-meridian reflecting Schmidt telescope (Zhao et al. 2012; Cui et al. 2012) that is operated by the National Astronomical Observatories, Chinese Academy of Sciences. With a field of view of 20 deg<sup>2</sup> and 4000 fibers at its focal plane, LAMOST can obtain up to 4000 spectra in one exposure and it has been the most efficient telescope for spectral acquisition in the world. Up to July 2018, LAMOST has completed its pilot survey and the first six years of regular survey which was initiated on September 2012. After the six-year-survey, the whole data (DR6) were released in 2018, containing 9,911,337 low-resolution spectra. They are flux(relatedly)- and wavelength-calibrated, sky-subtracted and have a resolution of  $R \sim 1800$  at 5500Å and a wavelength coverage of  $3700\text{Å} \leq \lambda \leq 9000\text{Å}$ . Each spectrum is spliced by the blue part and the red part. The integration time is 600, 1500 or 1800 seconds. All the low-resolution spectra were generally classified into different types through the pipeline including 9,231,057 stellar spectra, 177,270 galaxy spectra, 62,168 quasar spectra, and 440,842 spectra marked as unknown. The massive spectral database obtained by LAMOST is a rich resource for us to identify different kinds of peculiar stars. As CVs are one kind of valuable objects, searching them from the massive database is of much importance. And a larger CV catalogue is greatly helpful for follow-up studies.

## 3. METHOD

We first introduce a machine learning algorithm called UMAP for screening out the spectra with prominent H $\alpha$  emission features, which leads to a total of 169,509 spectra. The sample data used for supervised machine learning comes from 10 published CV or X-ray binary catalogues which are: Downes & Shara (1993); Downes et al. (1997); Downes et al. (2001); Szkody et al. (2011); Jiang et al. (2013); Breedt et al. (2014); Coppejans et al. (2016); Han et al. (2018); Ritter & Kolb (2003); Hou et al. (2020). The PyHammer v2.0 program is introduced to fit the LAMOST low-resolution spectra to help the manual inspection. There are two rounds in our

manual inspection. In the first round, those spectra of late-type main-sequence stars with enhanced chromospheric activities are removed. In the second round, we identify the early-type emission-line stars, pre-main-sequence, and other types of non-CV emission-line objects. For the left, we finally picked out the potential CV candidates.

### 3.1. $H\alpha$ classification based on machine learning

As the  $H\alpha$  is common to be an emission line for CV spectra, we first screen out the spectra with  $H\alpha$  emission features from the whole LAMOST DR6 database.

#### 3.1.1. Training sample

To obtain initial samples for supervised machine learning, we first cross-match the above mentioned 10 published catalogues with the LAMOST DR6 database. We manually examine each of the spectra in the cross-matching result and remove those that do not show  $H\alpha$  emission features. Thus, we obtained 392 spectra with  $H\alpha$  emission features. Note that not all these spectra are actually CVs, as long as they show  $H\alpha$  emission features. The wavelength range 6530-6600 Å of these spectra are extracted out as an input to the machine learning program (see Figure 1.) In order to avoid loss of CVs during outbursts, those spectra that have  $H\alpha$  wide absorption with emission cores are included in the sample. The double-peaked  $H\alpha$  profile is also included in the sample.

Then we randomly select 1000 spectra in the whole LAMOST DR6 database. We manually check the  $H\alpha$  line features, retaining those without typical  $H\alpha$  emission features, and obtain 973 spectra that can be used as controls in the supervised machine learning.

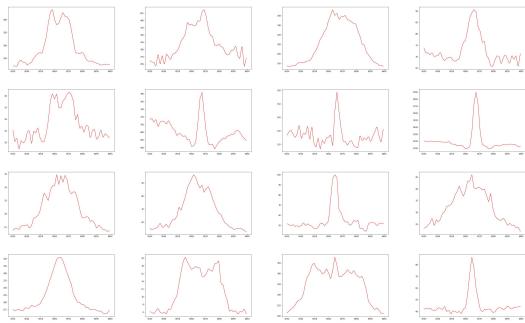


**Figure 1.** These are 16 examples of 392 sample spectra that are used for machine-learning training. The wavelength segment 6530-6600 Å associated with the  $H\alpha$  emission line is extracted out and used to screen for the same  $H\alpha$  emission line features.

#### 3.1.2. UMAP with k-NN algorithm

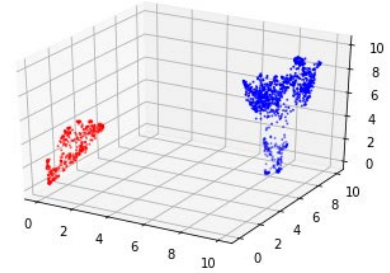


**Figure 2.** After dimension reduction by UMAP to 3 dimensions, 392  $H\alpha$ -emission spectra and 973 randomly selected spectra without  $H\alpha$  emission can be separated clearly.

Uniform Manifold Approximation and Projection (UMAP) is a novel machine-learning algorithm for dimension reduction proposed by McInnes et al. (2018), which is based on the mathematical framework of Riemannian geometry and algebraic topology. UMAP tends to preserve more of the global structure in dimension reduction while many other algorithms like PCA (Principal Components Analysis) seek to preserve the distance structure within the data. UMAP is also capable of preserving the local fine structure while still retaining much of the large-scale global structure like how PCA does. Thus, UMAP has natural advantages for dimension reduction of nonlinear data. Through our tests, the PCA algorithm often has the problem that the classification boundary in parameter space is not clear in comparison with the result of the UMAP algorithm, and may cause large contamination. Moreover, UMAP also shows superior run time performance for high-dimensional massive data compared to PCA. We therefore select UMAP as the dimension reduction algorithm for the high-dimensional spectral data. K-Nearest Neighbour (k-NN) is a common machine learning classification algorithm. The k-NN classifier is utilized to classify the data after the dimension reduction.

After training with the selected samples and testing several groups of parameters in the UMAP with k-NN algorithm, 392 sample spectra with  $H\alpha$  emission features and 973 without  $H\alpha$  emission features can be clearly separated in the three-dimensional space, as shown in Figure 2. The same algorithm is applied to all spectra in the LAMOST DR6 database, and we obtain a total of 169,509  $H\alpha$ -emission spectra. After we conduct a five-fold cross-validation (Shao 1993), we obtain a classification accuracy of over 99.6% in the cross-validation set.

### 3.2. PyHammer v2.0

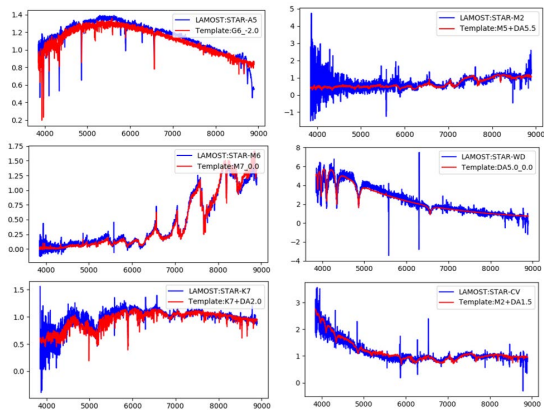


**Figure 3.** Examples of spectral fitting results obtained by using the Pyhammer v2.0 program. We use such spectra to identify the continuum and screen out the late type main sequence stars affected by chromosphere activity.

The PyHammer v2.0 program was published by [Roulston et al. \(2020\)](#) to give a more accurate classification of stellar spectra. We introduce this program to obtain the optimal fitted spectra as a reference for our manual inspection. We have modified the code to fit the LAMOST low-resolution spectra while still use the original templates. In the first round of manual inspection, those spectra that can be fitted well to the G/K/M-type templates considered as normal main-sequence stars with enhanced chromospheric activities, are removed. The spectra of this kind make up about half of the total 169,509 H $\alpha$ -emission spectra. After removing the chromospherically active stars from the first round, we go through the rest of the spectra to finally pick out CV candidates. Figure 3 shows some examples of the spectral fitting using PyHammer v2.0.

### 3.3. Manual inspection

#### 3.3.1. CV features

Typical CV spectra show a high-temperature continuum superimposed with strong emission lines, which are mainly Balmer and He I/He II lines. An important feature is that the line width of Balmer and helium emission lines appear to be significantly broad in most CV spectra, i.e. 70 Å for H $\alpha$ . Thus the existence of uniformly broad Balmer and He I/He II emission lines is a general criterion to identify CVs. The CV spectra usually do not have a steep decrement towards the higher order of the Balmer series as they can be seen up to H8 or higher. The strongest Balmer line may usually be H $\alpha$  to H $\delta$ . The line width of the helium emission lines is usually close to that of the Balmer lines. The double-peaked line profiles present in the Balmer and He emission lines indicate the existence of a rotating accretion disk. According to [Knigge et al. \(2000\)](#), when the disk is self-

occulted, the double-peaked emission lines tend to be narrower and straighter, which may be the reason of the straight double-peaked profiles in some CV spectra. In some cases, the Ca II H/K and Ca II triple lines also show broad emission, and the superposition of Ca II H and He lines make He appear stronger (close to or beyond H $\delta$ ) than it originally is. Moreover, when a spectrum is dominated by the companion’s contribution (often a M-type spectrum), the blue continuum would show an excess compared to the single M-type star. However, it is possible that at certain orbital phases the emission lines are obscured due to the eclipses, so that the spectrum does not show any CV feature. For very rare cases such as AM CVn systems, they do not have hydrogen lines due to the hydrogen-deficient nature.

For those spectra observed during outbursts, the Balmer lines show absorption through optically thick materials. The central emission cores can be absent at outburst peak and become larger if the spectrum is slightly past outburst. The central emission cores often present in all visible Balmer series, and the H $\alpha$  emission core is usually strong enough to maintain higher than the continuum (this can be called a core emission). The He I lines are also affected by wide absorption, while in many cases He II  $\lambda$ 4686 is still an emission line. During outbursts, He I  $\lambda$ 6678 behaves similarly to H $\alpha$  which usually shows emission and higher than the continuum. In some rare cases, the absorption lines are very strong, which cause the emission core of He I  $\lambda$ 6678 to be lower than the continuum.

Although in some cases the Balmer emission lines can be quite narrow, asymmetric broadening components can be found at the line wings that meet our empirical criteria of 24 Å, thus the spectra can be classified as CV candidates. Some of these cases belong to the AM Her-type CVs, for which the TiO absorption bands from the companion can be identified in low states. As mentioned in [Warner \(2003\)](#), the spectral lines in AM Her-type CVs can display a combination of a broad ‘base’ component and narrow components due to a combination of contributions of emission in the stream and pole regions. We find that the known AM Her-type CVs can be identified by the complex line structures and the profile differences between Balmer lines. The emission lines of AM Her-type CVs are more complicated than those of IPs. Strong He II  $\lambda$ 4686 lines are common in NLs and magnetic CVs. For AM Her-type CVs, He II  $\lambda$ 4686 are often stronger than or comparable to H $\beta$ . However, in the spectra of some known AM Her-type CVs, He II lines including He II  $\lambda$ 4686 are very weak or absent. Accordingly, He II lines are significant in the spectra of the known IPs (the strength ratio of He II  $\lambda$ 4686/H $\beta$   $\geq$

0.5, or He II  $\lambda 4686$  is close to but slightly weaker than  $H\beta$ ). In NLs, the relative strength of C III/N III  $\lambda 4560$  to He II  $\lambda 4686$  emission lines is generally greater than that in magnetic CVs, and in some cases, C III/N III  $\lambda 4560$  emission lines are as strong as He II  $\lambda 4686$ . Also, the emission lines of NLs can be narrower during low states than in higher states (Rodríguez-Gil et al. 2020). As C II emission lines appear commonly in NLs but not in DNs, the presence of C II lines can be an important feature to distinguish between the NL and the DN subclass.

More spectral line features of different subtypes of CV from the LAMOST observations have been described in Hou et al. (2020). For the manual inspection, the empirical criteria we chose to identify the potential CVs are listed below:

- The apparent line width of  $H\alpha$  is greater than or equal to  $24 \text{ \AA}$ ,
- He I  $\lambda 6678$  emission line presents in the spectra and it is not too narrow (less than  $14 \text{ \AA}$ ) compared to  $H\alpha$ ; or other He emission lines present,
- Balmer series or He lines show double-peaked profiles,
- Balmer series show wide absorption with emission cores and the emission cores can be seen at the Balmer series higher than  $H\gamma$ .

Satisfying any of the above criteria will allow us to mark it out in the manual inspection process. For low signal-to-noise ratio (SNR) spectra, when limited Balmer series or only the  $H\alpha$  emission line can be identified visually, they will be included as a CV candidate.

### 3.3.2. Inspection process

Each of the 169,509 spectra obtained from the machine learning program has been inspected manually in two rounds. In the first round, we remove the chromospherically active main-sequence stars (which can be fitted well to the G/K/M-type templates) by visually checking the whole spectra. In this process, we compare the LAMOST spectra with the fitted template by PyHammer v2.0 program to check whether there is an excess at the blue end. The remaining spectra, including those well-fitted to the O/B/A/F-type templates and binary star templates, as well as those not well-fitted to the templates (many CVs fall into this category), are retained for the second round. In the second round, we visually check the detailed spectral features carefully and single out those spectra that have CV features. Near the galactic plane, stellar spectra may be affected by the H II regions. By examining the presence of He absorption lines, we can remove the contaminations of the

Oe/Be stars. By judging the line width of  $H\alpha$ , we can remove the H II regions.

## 4. RESULTS

Finally, we obtained 475 spectra for 323 objects in total from LAMOST DR6. After checking the SIMBAD database, we find 271 known CVs or CV candidates, and 52 objects are new.

### 4.1. Distribution

The spatial distribution of the identified CVs is shown in Figure 4. The upper diagram is in equatorial coordinate, while the lower diagram is in galactic coordinate. For the 224 objects identified by Hou et al. (2020) from LAMOST DR5, our results cover 215 of them, and nine of them are not recovered in our results. In Section 4.2, we will specifically discuss why these nine objects are not included in our results. From Figure 4, we can see that the known CVs in LAMOST DR6 v2 are distributed evenly in space. The new CV candidates are more abundant near the galactic plane; however, they are especially rare in the northern galactic latitudes. Figure 5 shows the SNR distributions in  $g$  and  $i$  band for the LAMOST data. We can see that with our method, we have found more CV candidates with lower SNRs than those of Hou et al. (2020) in LAMOST DR6.

### 4.2. Cross-match with Hou et al. 2020

Hou et al. (2020) have presented 245 CV candidates from LAMOST DR5 and 224 objects are found in LAMOST DR6 v2 by cross-matching the coordinates. Out of these 224 objects, we have 215 objects in common with Hou et al. (2020) and nine objects are not included in our results (see Figure 6). We give the reasons why we lost these nine objects.

The spectrum of J0117 is affected by the bad quality. The red part is flat and does not have any feature, while the blue part shows an abnormally violent change. Therefore, in our manual inspection, we consider this spectrum unreliable and don't include it in our results.

J1234 is the prototype star and is a representative of the AM CVn-type systems with hydrogen-deficient. Due to the lack of  $H\alpha$  emission, our results do not include this type objects. The two spectra of this object do not show visible hydrogen lines on the high-temperature continuum, and He I lines on the blue part show broad absorption with partial filling at the center.

J0403 has two spectra in which the Balmer lines show deep absorption with emission cores, and He I lines show weak emission cores. Because the  $H\alpha$  emission core does not exceed the continuum, the UMAP algorithm failed to screen it out, but it can be a CV candidate as the

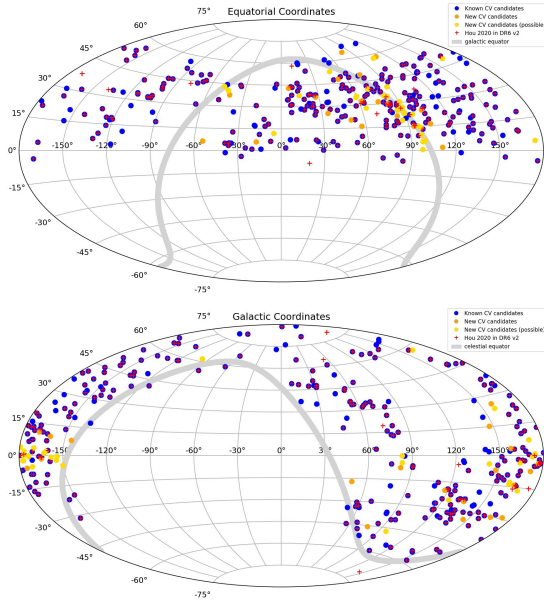


**Figure 4.** Spatial distributions of our results drawn in equatorial coordinates and galactic coordinates respectively. The blue spots represent 271 known CV objects from our analysis of LAMOST DR6 v2. The orange spots are 20 confirmed new CV candidates in our results and the yellow spots are 32 possible new CV candidates. The red cross markers indicate the 224 objects which are from cross-matching the result of Hou et al. (2020) with LAMOST DR6 v2.

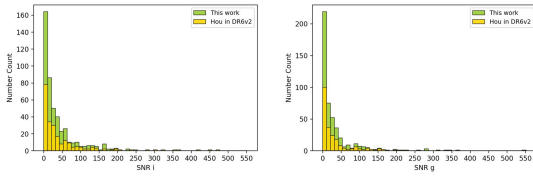


**Figure 5.** SNR distributions of g and i band. The green bars represent all 475 spectra in our result. The yellow bars represent the 220 spectra which are from cross-matching the result of Hou et al. (2020) with LAMOST DR6 v2.

Balmer emission cores exist up to H8 and He emission lines are marginally visible.

The spectrum of J1446 shows a component of a white dwarf on the blue part and a M-type companion on the red part, and it is fitted to the M3+DA2.5 template by the PyHammer program. Because its  $H\alpha$  line shows an emission core that does not exceed the continuum, the UMAP algorithm fails to identify it.

J1844 is a known dwarf nova, showing strong absorption with emission cores for both Balmer and He I lines. Its  $H\alpha$  line appears to have multiple components, and the emission core at the center is below the continuum so the UMAP algorithm fails to identify it.

The Balmer lines in the spectrum of J0043 show strong absorption.  $H\beta$  and higher members of Balmer series are

partially filled up by emission components, while the  $H\alpha$  is fully filled in so the UMAP algorithm fails to identify it as a CV. The He emission lines are barely visible.

J0331 is a known dwarf nova. The only spectrum shows very weak Balmer emission lines and the He lines are almost invisible. As the spectrum can be fitted to the M4 main-sequence template and does not show an excess on the blue end, we cannot identify it as a CV from this spectrum.

One of the spectra of J0439 can be fitted with the M6 template. The narrow Balmer emission lines may come from chromospheric activities. The other two spectra of this object show an indistinctive excess on the blue part, and they lack He lines, so we do not include the object in the manual inspection process. But it can still be a possible CV candidate as it presents enhanced Balmer emission lines and excess on the blue part compared with the template.

The spectrum of J0712 does not show an excess on the blue end relative to the M5 template, so we do not include it in the manual inspection process. But the enhanced Balmer emission and absorption center at higher Balmer lines still make it a possible CV candidate.

In conclusion, constrained by our machine learning samples, the UMAP algorithm has some limitations to perfectly classify the spectra that have strong wide absorption in  $H\alpha$  line with weak emission cores. If the spectra are dominated by the main-sequence star and they don't show an excess on the blue part or any obvious emission lines, we can not identify it as a CV in the manual inspection process. This phenomenon may be due to high inclination and specific orbital phases, which is relatively rare for CVs. In addition, a few spectra are affected by bad quality or very low SNRs. We considered them not trustworthy in the manual inspection and hence do not include them.

#### 4.3. Cross-match with other catalogues

We examine the cases which were previously classified as CV objects but are not included in our results from analysis of the LAMOST spectra. We cross-match the catalogs from the literature listed in section 3.1.1 with LAMOST DR6. From the cross-matching result, a total of 230 objects are classified as CVs or CV candidates in the SIMBAD database, in which 193 objects are found by us. For the rest 37 objects, three objects show CV features in their LAMOST spectra, and are described as follows. J1234, the prototype star of the hydrogen-deficient AM CVn system, and the dwarf nova J1844 have been explained in Section 4.2. J0713 (ASASSN-14mv) is also an AM CVn-type object (Denisenko et al. 2014), which shows strong He I and He II emission lines

but doesn't show hydrogen lines in its spectrum. The other 34 objects do not show features that could be identified as CVs in their LAMOST spectra, though they have been identified by spectroscopy or photometry. The likely reason is that they are too faint or in a fainter state that LAMOST can not obtain relatively high SNR spectra. Also, it is possible that the emission regions are obscured, or they were incorrectly identified as CVs in the catalogue (e.g. 2MASS J01095921+2801244 in [Downes et al. \(2001\)](#)).

#### 4.4. *New CV Candidates*

In our result, 52 objects are newly identified as CV candidates. Among them, 20 objects that can be classified as CVs as they show broad Balmer and He emission lines, are listed in Table 1. The other 32 objects, which can be classified as possible CV candidates, are listed in Table 2, as they lack some of the distinct features of CVs, or the spectra may be affected by abnormal circumstances, or they have a lower SNR. The 21 spectra of 20 confirmed CVs and 52 spectra of 32 possible CV candidates are plotted in Figures 10 and 11 in the Appendix, respectively.

#### 4.5. *Catalogue Description*

The 20 new confirmed CVs are presented in Table 1, while the 32 new possible CV candidates are shown in Table 2. In Table 3, we present the 271 previously known ones. The first two columns of each table are the LAMOST obsid (a unique spectra ID) and designation. The 16 spectra from LAMOST DR6 v1 which no longer exist in LAMOST DR6 v2 are marked by an asterisk before their obsid number. Column (3)-(5) are the MJD, right ascension and declination, respectively. Columns (6)-(8) are the CV subtype identified by us, [Hou et al. \(2020\)](#), and from SIMBAD, respectively. We mark all the new CV candidates with a single asterisk and label the 52 spectra of 32 new possible CV candidates as 'CV?' in column (6). If a source has more than one spectrum but those spectra do not show CV characteristics, we leave the row blank in column (6). Columns (9) and (10) are the median magnitude and the magnitude difference between the maximum and minimum taken from the ZTF DR4 data, respectively. The ZTF data are obtained by best cross-matching coordinates within 2 arcsec.

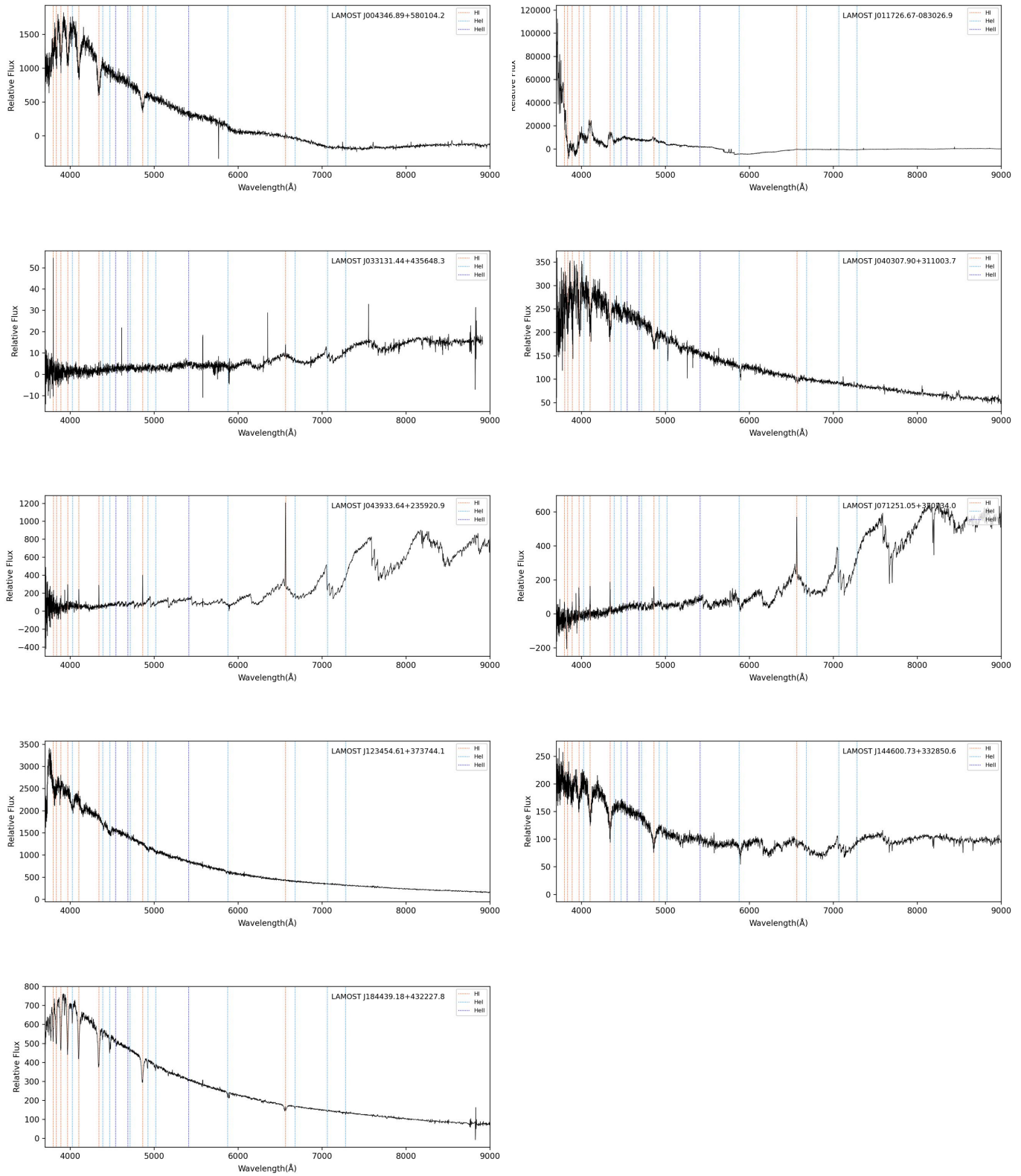


**Figure 6.** Spectra of nine objects from the catalogue of Hou et al. (2020) but are not found in our result. The wavelength range is from 3700 Å to 9000 Å.

Table 1. New confirmed CVs from LAMOST DR6

obsid	designation (LAMOST)	mjd	ra	dec	subtype <sup>a</sup> (this work)	subtype <sup>b</sup> (Hou2020)	subtype <sup>c</sup> (SIMBAD)	medianmag <sup>d</sup> (ZTF)	magdifference <sup>e</sup> (ZTF)
472302069	J002356.46+424707.8	57687	5.985285	42.7855	*DN_burst		none		
354712003	J014841.06+363350.0	57281	27.17111	36.56389	*DN_burst		15.68463	0.52242	
371007239	J014841.06+363350.0	57309	27.17111	36.56389	*DN_burst		none		
600008212	J021633.89+251346.5	58067	34.14122	25.22961	*MCV(polar)		18.80127	1.86958	
353714066	J032034.51+203607.2	57278	50.14383	20.602	*MCV(polar)		none		
587803184	J032641.99+475344.6	58018	51.67497	47.89573	*MCV(polar)		18.19204	2.89637	
605413195	J034713.84+161108.2	58074	56.80769	16.18563	*CV		16.91274	4.93641	
203507028	J040901.83+323955.6	56660	62.25766	32.66547	*NL		14.66591	0.60534	
631412182	J045452.12+491709.2	58135	73.71717	49.28589	*NL		17.20238	5.18567	
642708209	J045745.94+312517.2	58156	74.44143	31.42146	*NL		17.7648	0.92789	
593404034	J051949.51+642921.6	58045	79.95633	64.48935	*NL		17.29306	1.69211	
19714085	J052346.16+295034.5	55917	80.94235	29.84292	*CV		17.48023	0.13482	
198710203	J053532.64+220006.8	56652	83.88601	22.0019	*CV		19.52661	1.4481	
400115034	J061249.27+150642.1	57391	93.20533	15.11172	*DN_burst		17.73853	0.33707	
108714229	J065237.19+243622.1	56309	103.155	24.60617	*CV		15.70214	1.40907	
422415102	J070133.82+161010.3	57427	105.3909	16.16954	*DN_burst		18.35857	4.36762	
631513222	J071553.88+581606.4	58135	108.9745	58.26846	*MCV(IP)		16.17882	1.2921	
600414109	J072304.77+020437.4	58067	110.7699	2.077058	*NL		15.48614	0.38905	
587208191	J202300.37+063142.4	58016	305.7516	6.528447	*NL?		none		
593810181	J211249.93+374225.8	58046	318.2081	37.70719	*DN_burst		16.50493	0.41542	
173307033	J225017.79+060645.8	56598	342.5741	6.112739	*CV		16.19793	0.38934	

NOTE—

<sup>a</sup> If a source has more than one spectrum but the spectrum has no visible CV characteristics, we leave the row blank. If the row is the spectrum of a new CV candidate, we mark it with a single asterisk in this column. For new confirmed CV candidates, we particularly give the subtype inferred from the spectrum. Two poorly known objects discussed in section 5.2 are marked by double asterisks.

<sup>b</sup> The column is the CV subtype for the corresponding LAMOST DR6 spectra given by Hou et al. (2020).

<sup>c</sup> The column is the CV subtype from SIMBAD, or from the literature subtype given in the catalogue of Hou et al. (2020). If the source exists in SIMBAD but is given a type other than CV, it is marked as 'none'.

<sup>d</sup> This is the median magnitude taken from the ZTF DR4. The ZTF data is obtained by best matching within 2 arcsec with our result.

<sup>e</sup> This is the difference between the maximum and minimum magnitude taken from the ZTF DR4.

Table 2. New possible CV candidates from LAMOST DR6

obsid	designation (LAMOST)	mjd	ra	dec	subtype <sup>e</sup> (this work)	subtype <sup>b</sup> (Hon2020)	subtype <sup>c</sup> (SIMBAD)	medianmag <sup>d</sup> (ZTF)	magdifference <sup>e</sup> (ZTF)
18508092	J005651.51+375620.4	55914	14.21465	37.93903	*CV?		19.83481	0.52011	
16115150	J031108.31+530719.3	55910	47.78466	53.12206	*CV?				
181509193	J035603.23+351450.5	56617	59.01347	35.24738	*CV?		14.89156	1.63763	
212414002	J035603.23+351450.5	56684	59.01347	35.24738	*CV?				
182009193	J035603.23+351450.6	56617	59.01347	35.24741	*CV?				
194714002	J035603.23+351450.6	56645	59.01347	35.24741					
194716052	J035933.23+360323.1	56645	59.88847	36.05643	*CV?		14.9497	0.10124	
181912155	J035933.23+360323.1	56617	59.88847	36.05643					
182012155	J035933.23+360323.1	56617	59.88847	36.05643					
194616052	J035933.23+360323.1	56645	59.88847	36.05643					
194816052	J035933.23+360323.1	56645	59.88847	36.05643					
17506020	J041407.98+280120.3	55913	63.53326	28.02231					
119012144	J041407.98+280120.3	56331	63.53326	28.02231	*CV?		15.74186	0.0913	
214612144	J041407.98+280120.4	56687	63.53325	28.02234					
214712144	J041407.98+280120.4	56687	63.53325	28.02234					
39906248	J044644.51+400141.0	55967	71.08547	40.02806	*CV?		14.14061	0.05539	
68812240	J052443.05+350123.3	56219	81.17938	35.02314	*CV?		18.15303	1.49098	
269314147	J053416.07+342316.1	56981	83.567	34.38782	*CV?				
132413240	J053416.08+342316.1	56358	83.567	34.38781	*CV?		15.34793	0.1759	
300813240	J053416.08+342316.1	57042	83.567	34.38781	*CV?				
16202089	J054311.80+254445.8	55910	85.79917	25.74608	*CV?		14.88737	0.11771	
81412213	J054311.80+254445.8	56254	85.79917	25.74608	*CV?		14.88737	0.11771	
406715055	J054345.28+252601.0	57400	85.93869	25.43363	*CV?		17.47745	0.10737	
108002166	J054627.34+190011.9	56308	86.61396	19.00333	*CV?		13.49713	0.09616	
81116232	J055303.79+262659.4	56253	88.26582	26.44984	*CV?		20.81788	1.02977	
124105039	J055444.33+401846.5	56343	88.68471	40.31292	*CV?		14.74165	0.1076	
83211001	J055444.33+401846.5	56256	88.68471	40.31292					
124405039	J055455.84+401952.3	56343	88.73269	40.33121					
83111007	J055455.84+401952.3	56256	88.73269	40.33121	*CV?		14.94291	0.19556	
116308162	J055834.38+232004.9	56321	89.64327	23.33472					
116308163	J055924.27+233707.6	56321	89.85116	23.61878	*CV?		15.45488	0.11825	
81108248	J055924.73+234341.1	56253	89.85307	23.72811	*CV?		14.19076	0.12284	
11107016	J060116.87+271327.1	55898	90.32029	27.22422	*CV?		19.08045	1.30034	
127912024	J060214.93+303536.8	56349	90.56224	30.59356	*CV?		18.20835	0.12946	
485106105	J062104.00+221554.7	57720	95.2667	22.26522	*CV?		14.32692	0.10813	
486306105	J062104.00+221554.7	57723	95.2667	22.26522	*CV?				
486806105	J062104.00+221554.7	57724	95.2667	22.26522	*CV?				

Table 2 continued

Table 2 (continued)

obsid	designation (LAMOST)	mjd	ra	dec	subtype <sup>a</sup> (this work)	subtype <sup>b</sup> (Hou2020)	subtype <sup>c</sup> (SIMBAD)	medianmag <sup>d</sup> (ZTF)	magdifference <sup>e</sup> (ZTF)
497206105	J062104.00+221554.7	57739	95.2667	22.26522	*CV?				
506606105	J062104.00+221554.7	57718	95.2667	22.26522	*CV?				
508806105	J062104.00+221554.7	57757	95.2667	22.26522	*CV?				
509806105	J062104.00+221554.7	57758	95.2667	22.26522	*CV?				
510706105	J062104.00+221554.7	57759	95.2667	22.26522	*CV?				
603206105	J062104.00+221554.7	58076	95.2667	22.26522	*CV?				
606206105	J062104.00+221554.7	58075	95.2667	22.26522	*CV?		14.57116	0.03718	
615306105	J062104.00+221554.7	58098	95.2667	22.26522	*CV?				
617806105	J062104.00+221554.7	58104	95.2667	22.26522	*CV?				
620206105	J062104.00+221554.7	58108	95.2667	22.26522	*CV?				
631106105	J062104.00+221554.7	58134	95.2667	22.26522	*CV?				
644906105	J062104.00+221554.7	58161	95.2667	22.26522	*CV?				
483206105	J062104.00+221554.7	57715	95.2667	22.26522					
490506105	J062104.00+221554.7	57727	95.2667	22.26522					
501106105	J062104.00+221554.7	57748	95.2667	22.26522					
525406105	J062104.00+221554.7	57781	95.2667	22.26522					
529006105	J062104.00+221554.7	57787	95.2667	22.26522					
529606105	J062104.00+221554.7	57788	95.2667	22.26522					
280405205	J062549.60+145347.4	57006	96.45668	14.89651	*CV?		16.60911	0.40176	
101201021	J062811.33+004654.5	56295	97.04721	0.781809	*CV?		14.90546	0.08848	
419307028	J062842.43+093209.2	57422	97.17679	9.535889	*CV?		16.76195	1.77769	
44314014	J063018.87+053831.3	55983	97.57867	5.642036	*CV?		13.31386	0.10978	
442712204	J063018.88+053831.4	57468	97.57867	5.642059					
406804155	J063209.32+140334.5	57400	98.03886	14.05961	*CV?		18.28807	3.54584	
44515210	J063722.97+060755.8	55983	99.34572	6.132189	*CV?				
111003180	J065815.75+575142.9	56316	104.5656	57.86194	*CV?		16.01802	0.18338	
110903180	J065815.75+575142.9	56316	104.5656	57.86194					
217303180	J065815.75+575142.9	56699	104.5656	57.86194					
629705190	J104751.79+483503.7	58130	161.9658	48.58438	*CV?	none	18.48886	0.34744	
525913199	J113835.67+044454.7	57782	174.6486	4.748538	*CV?	none	19.32805	3.88678	
587910071	J204502.35+430520.6	58018	311.2598	43.08906	*CV?	none	15.39373	1.23171	
594305076	J210306.10+402306.3	58050	315.7754	40.38511	*CV?	none	17.1679	0.09375	
355016173	J233900.38+115707.2	57283	354.7516	11.95201	*CV?	none	18.19033	0.27358	

NOTE—

(This table is available in its entirety in machine-readable form.)

**Table 3.** Previously known CV candidates from LAMOST DR6 (examples of 15 rows)

obsid	designation (LAMOST)	mjd	ra	dec	subtype <sup>a</sup> (this work)	subtype <sup>b</sup> (Hou2020)	subtype <sup>c</sup> (SIMBAD)	medianmag <sup>d</sup> (ZTF)	magdifference <sup>e</sup> (ZTF)
266703059	J001204.51+020129.8	56977	3.018792	2.024947	CV	CV	none	16.5676	0.42809
592201085	J001856.93+345444.2	58039	4.737242	34.91228	CV	CV	CV	17.27818	0.7825
592301085	J001856.93+345444.2	58039	4.737242	34.91228	CV	CV	CV	17.27818	0.7825
614101085	J001856.93+345444.2	58095	4.737242	34.91228	CV	CV	CV	17.27818	0.7825
75902147	J002148.44+350451.1	56231	5.45187	35.08089	CV	CV	CV	14.51631	0.88123
284616096	J002148.44+350451.1	57014	5.45187	35.08089	CV	CV	CV	14.51631	0.88123
592307039	J002148.44+350451.2	58039	5.451867	35.08089	CV	CV	CV	14.51631	0.88123
614107039	J002148.44+350451.2	58095	5.451867	35.08089	CV	CV	CV	14.51631	0.88123
76002147	J002148.45+350451.1	56231	5.451892	35.08088	CV	CV	CV	14.51631	0.88123
81816096	J002148.45+350451.2	56254	5.451877	35.08091	CV	CV	CV	14.43212	0.90129
81916096	J002148.45+350451.2	56254	5.451877	35.08091	CV	CV	CV	14.43212	0.90129
*174106175	J002500.18+073349.3	56601	6.250776	7.563698	CV	CV	CV	19.15958	3.25442
483901014	J002842.53+311819.4	57716	7.177215	31.3054	CV	CV	CV	18.73505	2.02
82609065	J003005.80+261726.3	56255	7.524205	26.29067	CV	NL-candidate	NL	15.2266	5.27938
90111206	J003135.88+434905.3	56265	7.899519	43.81814	CV	CV	Nova	15.67982	0.20626
...	...	...	...	...	...	...	...	...	...

NOTE—  
(This table is available in its entirety in machine-readable form.)

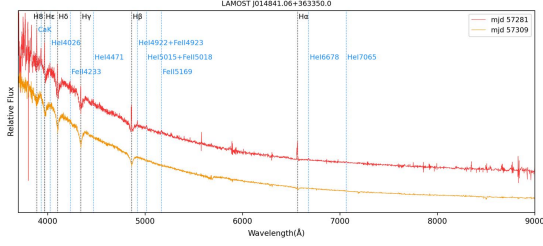


**Figure 7.** Two spectra of J0148 with MJDs 57281 and 57309, respectively, show variation. The wavelength range is from 3700 Å to 9000 Å. The upper red line represents the spectrum of MJD 57281, while the lower orange line for MJD 57309. The Balmer lines are indicated with dotted black lines, and the He I, He II and Fe II lines are indicated with dotted blue lines.

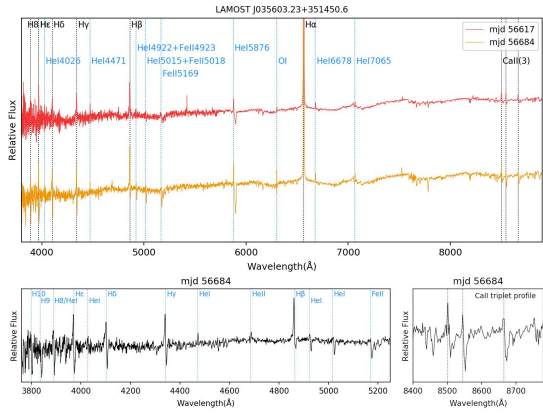


**Figure 8.** Upper panel: Two spectra of J0356, taken on MJDs 56617 and 56684, respectively. The upper red line represents the spectrum of MJD 56617, while the lower orange line for MJD 56684. The Balmer lines are indicated with dotted black lines, and the He I, He II and Fe II lines are indicated with dotted blue lines. The wavelength range is from 3800 Å to 8900 Å. Lower panel: the blue part and the Ca II triplet region of the spectrum of MJD 56684 show the anti-P Cyg profile.

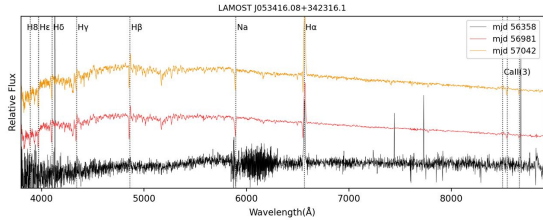


**Figure 9.** Three spectra of J0534+3423 are taken at MJDs 56358, 56981 and 57042, respectively. The black, red and orange lines represent the spectrum taken at MJDs 57042, 56981 and 57042, respectively. The lines of Balmer series, Na  $\lambda$ 5895.6 and Ca II triplets are indicated with dotted black lines. The wavelength range is from 3800 Å to 8900 Å.

## 5. DISCUSSION

### 5.1. Objects of New CV Candidates

Among the new CV candidates, we find some of them showing interesting features and discuss them in the following subsections according to their subtypes.

#### 5.1.1. DN in outburst

J0148, J0612, J0701, J0023, and J2112 reveal typically spectral features of DNs undergoing outbursts, and the wide absorption is visible in each Balmer line in the spectra of these objects. We note that the Balmer lines for J0148, J0612, J0701, and J2112 are narrow, for example, the H $\alpha$  is less than 24 Å, while J0023 shows slightly broad emission components (the H $\alpha$  emission core is 33 Å). Asymmetric central absorption also presents at the Balmer emission cores in all the spectra.

There are two spectra of J0148 (Figure 10 on page 19). The emission of the Balmer series is significant in the middle of the wide absorption lines, while He I lines are in emission and does not exhibit wide absorption features. Thus, we can identify it as a DN in outburst. The other spectrum mainly shows wide Balmer absorption lines. The variations of the two spectra observed at different times are shown in Figure 7. The spectrum of MJD 57281 presents central emission cores of Balmer lines, while H $\alpha$  and He I  $\lambda$ 6678 are almost pure emission. In the spectrum of MJD 57309, the Balmer lines become nearly all absorption, while the H $\alpha$  still presents an obvious emission core. Although the multiple emission components with asymmetric features are not obvious, they can be seen in the absorption lines of Balmer series higher than H $\alpha$ . This means that the emission components have a steeper decrement than those of the absorption. Besides, He I  $\lambda$ 6678 also shows very weak emission. For these features above, the spectrum of MJD 57309 is likely to be taken during the outburst maximum (Warner 2003).

The spectrum of J0612 (Figure 10 on page 20) shows narrow asymmetric core emissions with weak wide absorption in the Balmer series, and the He I  $\lambda$ 4471,  $\lambda$ 5876,  $\lambda$ 6678,  $\lambda$ 7065 lines are also in emission.

In the spectrum of J0701 (Figure 10 on page 20), the absorption lines are strong while the emission cores are weak for the higher order Balmer series., and the He I  $\lambda$ 6678 line is affected by the absorption.

The spectrum of J0023 (Figure 10 on page 19) shows strong wide Balmer absorption with broad emission cores, and there seems to be two emission components of the Balmer lines. The He II  $\lambda$ 4686 is a strong emission line, and the C III/N III blend at 4650 Å is also in emission, which may indicate the presence of a hot emission zone in the disk.

The spectrum of J2112 (Figure 10 on page 20) shows weak wide absorption of Balmer lines, while the weak He I  $\lambda 6678$  line presents emission. The C III/N III blend at  $4650 \text{ \AA}$  is in emission, while He II is absent. Note that Fe II lines are present in all of the spectra above.

#### 5.1.2. *Nova-like type*

J0409, J0519, J0723, J0454, and J0457 mainly show strong C III/N III emission features and C II lines, resembling the NL subtype of CVs. The common central absorption or double-peaked profile in the emission lines suggests the presence of disks.

J0409 (Figure 10 on page 19) presents peculiar features of a high-temperature continuum along with obvious H $\alpha$ , H $\beta$ , He I, He II, C III/N III, and C II emission lines. The Balmer decrement is quite strong, and the asymmetric double-peaked profiles present. The He II  $\lambda 4686$  line and C III/N III blend are extremely strong, which are much higher than the apparent strength of H $\alpha$  and H $\beta$ . The strength of C III/N III is comparable to that of He II  $\lambda 4686$ . The Ca II H/K lines show single narrow absorption, which could be due to interstellar absorption. Interestingly, we find that J2023, which is also one of the newly discovered CV candidates, has very similar features, while the prominent difference is that in J2023 the He II  $\lambda 4686$  is absent, for which it can only be classified as a possible NL.

J0723 (Figure 10 on page 20) shows strong Balmer emission lines but weak He I lines. The Balmer lines show asymmetric shapes and the strongest Balmer line is H $\alpha$ . For H $\gamma$ , an absorption center is present which may indicate the existence of an accretion disk. The He II  $\lambda 4686$  is much weaker than H $\beta$ , while the C III/N III blend is as strong as He II  $\lambda 4686$ . The Ca II  $\lambda 3934$  line shows narrow absorption, while C II  $\lambda 7234$  is in emission.

J0454 (Figure 10 on page 19) shows very broad strong Balmer, He I, He II, and C II emission lines. The C III/N III is about half the height of that of He II  $\lambda 4686$ . The broad and asymmetric double-peaked shapes in the Balmer and He lines are significant, which indicates that there is an accretion disk.

The spectra of J0519 (Figure 10 on page 20) and J0457 (Figure 10 on page 19) have relatively low SNR. He II  $\lambda 4686$  emission can be identified in both spectra. The C III/N III emission possibly exists in J0519, while C II  $\lambda 7234$  emission is visible in J0457. For J0519, the central absorption is seen in the Balmer lines, which indicates there is an accretion disk.

#### 5.1.3. *Magnetic CVs*

Four new CV candidates, J0320, J0326, J0216, and J0715, can be classified as magnetic CVs by the strong He II emission and other spectral features.

J0320 (Figure 10 on page 19) shows strong broad Balmer emission lines, the strongest being H $\delta$ , and they are all blue-shifted. He II  $\lambda 4686$  is stronger than H $\beta$ . He I  $\lambda 7281$ ,  $\lambda 7065$ ,  $\lambda 6678$ ,  $\lambda 5876$ ,  $\lambda 4388$ ,  $\lambda 4471$  and  $\lambda 4026$  are in emission. The Na I D line shows very strong absorption, which may be contributed by the companion star. The C III  $\lambda 4634$  and C IV  $\lambda 5805$  lines also show emission. As He II  $\lambda 4686$  is strong and Balmer lines split, this object could be a magnetic CV, possibly of AM Her type.

J0326 (Figure 10 on page 19) reveals an M-type continuum at the red part along with very strong Balmer and He I/He II emission lines. Both the narrow and broad emission components in the Balmer and He II lines can be seen, and the strongest Balmer line is H $\delta$ . C II lines only show weak emissions. Deep Na I D absorption line can be seen at  $5895 \text{ \AA}$ . The strength of He II  $\lambda 4686$  is almost the same as H $\beta$ , and C III is nearly absent. The spectroscopic features are consistent with that of the AM Her systems.

J0216 (Figure 10 on page 19) shows a relatively flat continuum with strong Balmer and He I/He II emission lines. As the He II  $\lambda 4686$  emission line is stronger than H $\beta$ , and there are multiple components or splits in the Balmer lines, we classify it as a magnetic CV, possibly of the AM Her type.

J0715 (Figure 10 on page 20) shows broad Balmer emissions. The H $\alpha$  emission line presents a ‘wine bottle’ profile. The He II  $\lambda 4686$  line is quite strong as the strength is comparable to that of H $\beta$ , and the C III/N III blend also show strong emission. In view of the above characteristics, we consider that it as a possible magnetic CV, specifically an IP.

#### 5.1.4. *Binary spectra*

The spectra of J0523, J2250, J0535, J0628, J0356 and J2045 present dominant cool companion star features on the red part. For J2339 and J0311, both the companion and the white dwarf features can be seen.

The spectrum of J0523 (Figure 10 on page 20) presents strong narrow Balmer emission lines with weak decrement to higher order. The spectrum shows prominent M-type star features on the red part, and it can be fitted with a M2-type star. There is a significant excess at the blue part. The Balmer series present an asymmetric broadening component superimposing on the strong narrow emission. He I  $\lambda 6678$ ,  $\lambda 5876$ , and  $\lambda 4471$  lines are in emission, while He II lines are absent.

J2250 (Figure 10 on page 21) shows a continuum that can be fitted with a late K-type star, while presents strong Balmer, He I and He II emission lines. The Balmer lines have a broad component and show obvi-

ous asymmetric structure. The narrow Balmer emission components show a decrement, while the broad components do not show obvious decrement and shift to blue with respect to the narrow components. We consider that the narrow Balmer emission may come from chromospheric activities of the companion star, while the broad one come from an accretion disk or hot spot. In addition, the deep Na I D  $\lambda 5895$  absorption line as well as [O I]  $\lambda 6302$  and O I  $\lambda 6365$  absorption lines is visible.

J0356 (Figure 11 on page 22) has multiple spectra in LAMOST DR6, and shows prominent variations. We present two of the spectra of MJDs 56617 and 56684 in Figure 8. Both spectra show the M-type companion features along with strong Balmer and He I/He II emission lines. Compared with the fitted template spectrum, the relative flux of the LAMOST spectra has obvious excesses at the blue part. In the lower panel of the figure, the near-ultraviolet and near-infrared regions of the spectrum of MJD 56684 are shown. In the observation of MJD 56684, the Balmer series members higher than  $H\alpha$ , He I and Ca II lines all show anti-P Cyg profile, which reveals the explosive nature of the object, while He II  $\lambda 4686$  line appears to be a single emission or have a P Cyg profile. However, we can not completely rule out the possibility that it is an explosive pre-main-sequence object (like FU Orionis type stars) by the spectral features alone.

The spectra of J0535 (Figure 10 on page 20), J0628 (Figure 11 on page 26) and J2045 (Figure 11 on page 26) all show features of a M-type companion. In those spectra, the Balmer emission lines are quite narrow and all show asymmetric features, and the Ca II H/K lines are in strong emission. The  $H\beta$  is much weaker than  $H\alpha$ , which is not typical for CVs. Moreover, J0535 shows He I emission lines, while J0628 and J2045 show both He I and He II emission lines. The Ca II triplets at  $8500 \text{ \AA}$  present slight emission in the former two but strong in J2045. [O I]  $\lambda 6302$  also presents weak emission in all those spectra.

The spectrum of J2339 (Figure 11 on page 27) presents both a M-type companion and a white dwarf features. In the spectra, both  $H\alpha$  and  $H\beta$  show strong emission with double-peaked profiles, and He I  $\lambda 6678$  presents weak and broad emission, which may indicates that there is an accretion disk.

J0311 (Figure 11 on page 22) has been classified as a DA-type white dwarf by Zhang et al. (2013), and they suggested it has unknown emission process. The spectrum presents strong  $H\alpha$  emission core and has strong Balmer decrement for the emission components, while the broad Balmer absorption resemble a white dwarf. It also presents strong Ca II triplets but weak He I emis-

sion lines. As there are multiple emission components in the Balmer series and some are broad, we consider this object may have a CV nature.

#### 5.1.5. Other Objects

There are 21 spectra of J0621 in LAMOST DR6, and 15 of them show  $H\alpha$  emission features for which can be identified as a possible CV candidate, as shown in Figure 11 on pages 24 and 25. The  $H\alpha$  emission lines in its spectra present complex structure. There is a sharp flux increase at the blue end with emission features. Four spectra of this object taken before MJD 58076 show very wide absorption (the line width of  $H\alpha$  beyond  $130 \text{ \AA}$ ) of Balmer and Paschen series, and the Na I absorption lines are strong. Seven spectra taken at MJD 58076 and later show an unusual double hump at  $4000 \text{ \AA} - 5000 \text{ \AA}$  for unknown reasons. As these spectra are taken at different dates, the double hump feature should be real rather than instrumental problems.

J0534 is identified as a possible CV candidate due to the broad  $H\alpha$  emission feature. It has three spectra in LAMOST DR6 as shown in Figure 9. The spectrum of MJD 56358 has a relatively low SNR, in which only symmetrical  $H\alpha$  emission line can be seen. In the spectra of MJDs 56981 and 57042, a late G- to early K-type companion can be clearly seen. These two spectra present a strong P Cyg profiles for  $H\alpha$  to  $H\gamma$  and Ca II triplets, which could indicate the presence of disk winds or jets. However, in the spectrum of MJD 56981, both the strength ratio of Sr II  $\lambda 4077$  to Fe I  $\lambda 4046$  and the strength of C/N  $\lambda 4215$  band indicate that the K-type star resembles a giant rather than a main-sequence (Gray et al. 2009). The lack of He emission lines also suggests that it may not be a CV. Follow up observations are required to determine the nature of this object.

#### 5.2. Poorly investigated objects

J0631 was investigated by Balanutsa et al. (2013) using the MASTER-Tunka auto-detection system. Based on the blue color and photometric variability, it was identified as a probable dwarf nova. It has also a UV counterpart GALEX J0631. There are three spectra of this object. Although the SNRs are low for all of them, the DN properties can be found. In the spectrum of MJD 55861, the continuum reveals a high-temperature component, and the emission features of the Balmer and He lines are obvious. The Balmer core emissions are not so broad and may have multiple components, while the weak wide absorption can be seen for  $H\beta$  and higher Balmer series members. Strong He II  $\lambda 4686$  emission line also presents in the spectra. The above features are in consistent with a dwarf nova during an outburst. For the other two spectra of MJDs 55873 and 57096, the

continuum is quite flat. They both present distinctive asymmetric Balmer and He I  $\lambda 6678$  emission lines, while He II  $\lambda 4686$  is absent in the two spectra. We thus consider both spectra were taken at the quiescent phase of a DN.

J0720 has been identified to be most likely a polar with an extreme hot spot (Denisenko 2018), as it shows a large amplitude of variation presenting in its light curve with no eclipses found. It has an X-ray counterpart XMMSL2 J0720. There is only one spectrum in LAMOST DR6, which shows sharp and asymmetric Balmer emission lines with no obvious continuum. He I  $\lambda 4471$ ,  $\lambda 6678$ , and  $\lambda 7065$  emission lines also present while He II  $\lambda 4686$  is absent. These spectral features are consistent with those of a polar. However, the  $H\beta$  shows a double-peaked profile, which might imply the presence of a residual disk.

## 6. CONCLUSION

Using the UMAP with k-NN method, we have spectroscopically identified 475 CV spectra of 323 objects from LAMOST DR6, of which 52 objects are new. After cross-match with the DR5 CV catalogue presented by Hou et al. (2020), our results include 215 of their 224 objects in LAMOST DR6 v2. The other nine are not included as their spectra don't show obvious  $H\alpha$ -emission features. This is due to the limitations of the current UMAP method.

By visually examining the CV features of the spectra, we can remove contamination of the Oe/Be stars and H II regions, and identify more potential CV candidates that are previously difficult to single out. The new CVs include five DNs during outbursts, five NLs and four magnetic CVs (three of AM Her type and one of IP type). We also discuss objects that directly show the binary systems. In addition, we listed two objects that have been poorly investigated from the known CVs in our catalogue. Their spectral features confirm the sub-type they previously classified. Nevertheless, for J0720,

the  $H\beta$  presents an double-peaked profile which may suggest that there is a residual disk.

Our results show that the UMAP algorithm can identify CV spectra that present an core emission at  $H\alpha$ , however, there are still shortcomings if the emission core is weak, the program may not pick them out. More samples are needed for training of the UMAP method to improve the classification accuracy. Our results do not include the AM CVn type, and the pre-polars which may only show broad cyclotron emission lines, because they both lack hydrogen lines. New methods should be adopted to identify these two types of CVs as they may not have any  $H\alpha$  emission lines.

In the future, we will carry out follow-up photometric studies on the new CV candidates and poorly studied or interesting CV objects, obtain the orbital parameters to further study their properties.

## ACKNOWLEDGEMENTS

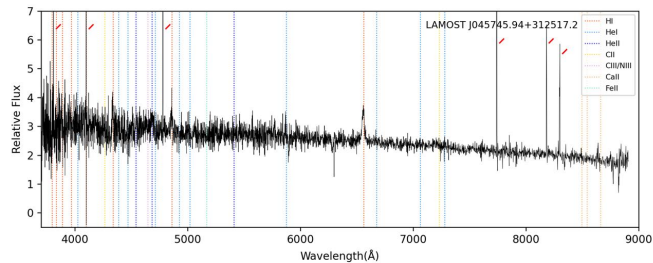
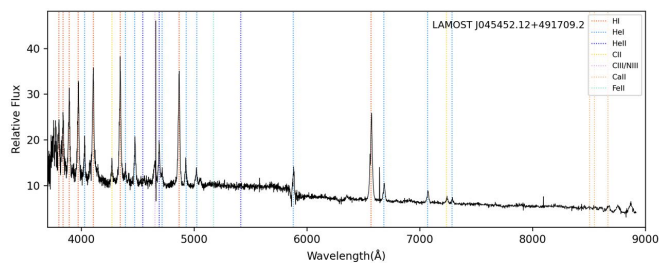
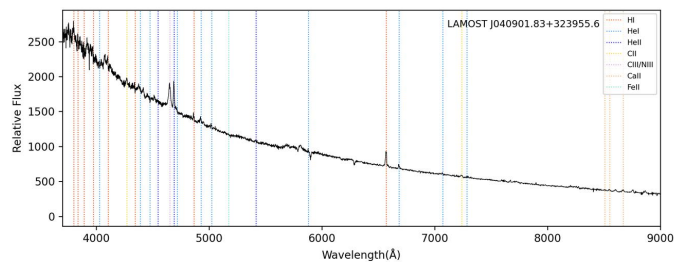
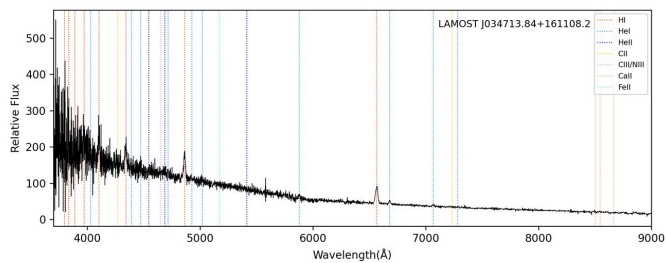
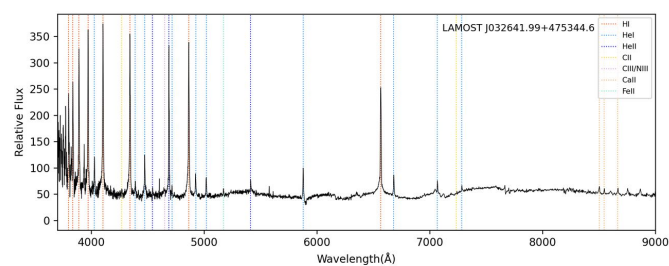
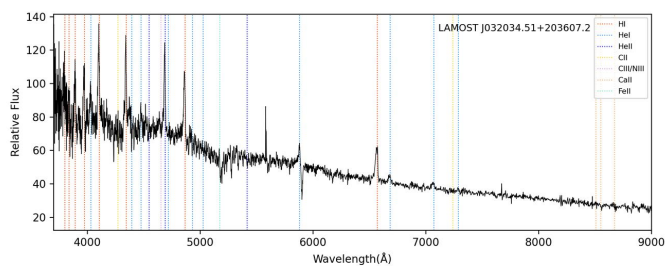
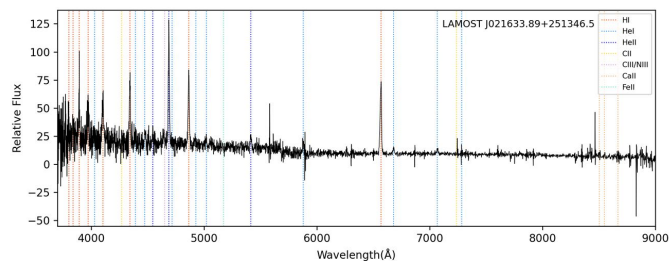
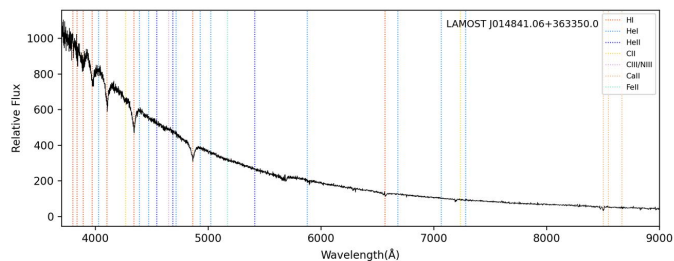
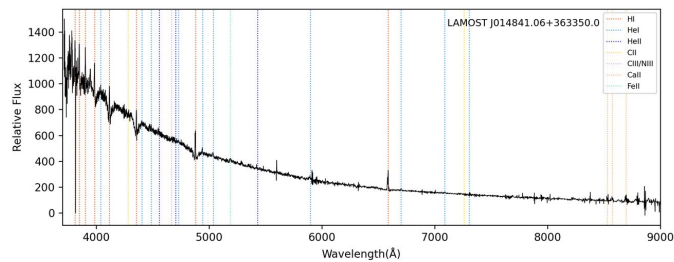
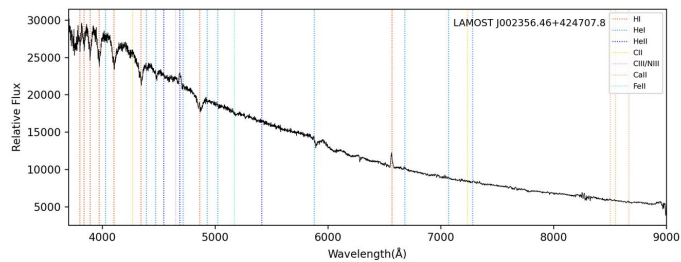
We would like to thank the anonymous referee for his/her very helpful feedback. This work is supported by the National Key Basic R&D Program of China via 2019YFA0405500, 2019YFA0405501, the National Natural Science Foundation of China (NSFC) under grant 11773009, 11673007, 12090040, 12090044, 11833006, 11903012, 11703038, 12033003 and 12173103, the Natural Science Foundation of Hebei Province under grants A2021205006. W.Y.C. is also supported by the '333 talents project' of Hebei Province. The Guo Shou Jing Telescope (the Large Sky Area Multi-Object Fiber Spectroscopic Telescope, LAMOST) is a National Major Scientific Project built by the Chinese Academy of Sciences. Funding for the project has been provided by the National Development and Reform Commission. LAMOST is operated and managed by National Astronomical Observatories, Chinese Academy of Sciences. We acknowledge the science research grants from the China Manned Space Project with NO.CMS-CSST-2021-A08. This research has made use of the SIMBAD database, operated at CDS, Strasbourg, France. This work has made use of data from the Zwicky Transient Facility (ZTF) data.

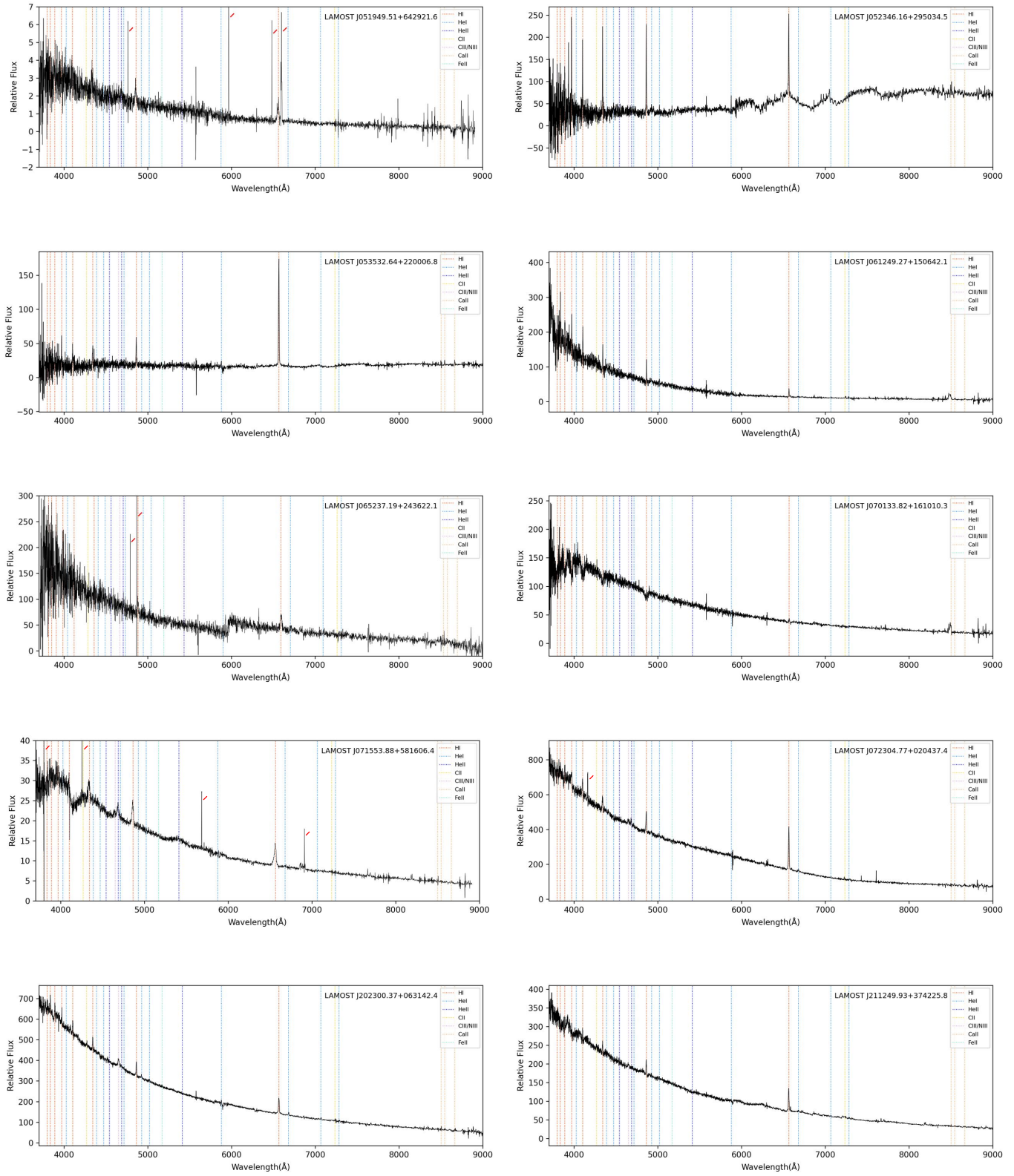
## REFERENCES

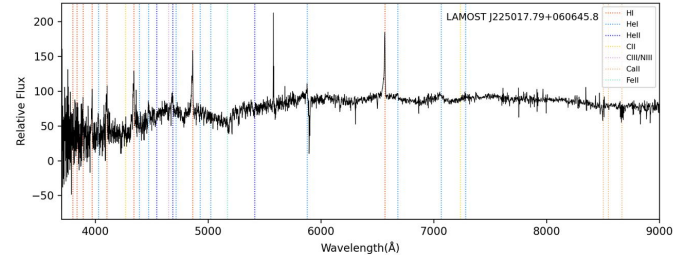
- Anupama, G. C. 2011, Proceedings of the International Astronomical Union, 7, 154–161, doi: [10.1017/S1743921312014913](https://doi.org/10.1017/S1743921312014913)
- Balanutsa, P., Denisenko, D., Gorbovskoy, E., et al. 2013, The Astronomer's Telegram, 5451, 1
- Breedt, E., Gänsicke, B., Drake, A., et al. 2014, Monthly Notices of the Royal Astronomical Society, 443, 3174
- Coppejans, D. L., Körding, E. G., Knigge, C., et al. 2016, Monthly Notices of the Royal Astronomical Society, 456, 4441
- Coppejans, D. L., Körding, E. G., Miller-Jones, J. C., et al. 2015, Monthly Notices of the Royal Astronomical Society, 451, 3801
- Cui, X.-Q., Zhao, Y.-H., Chu, Y.-Q., et al. 2012, Research in Astronomy and Astrophysics, 12, 1197

- Denisenko, D. 2018, *The Astronomer's Telegram*, 11626, 1
- Denisenko, D., Lipunov, V., Gorbovskoy, E., et al. 2014, *The Astronomer's Telegram*, 6857, 1
- Downes, R., Webbink, R. F., & Shara, M. M. 1997, *Publications of the Astronomical Society of the Pacific*, 109, 345
- Downes, R. A., & Shara, M. M. 1993, *Publications of the Astronomical Society of the Pacific*, 105, 127
- Downes, R. A., Webbink, R. F., Shara, M. M., et al. 2001, *Publications of the Astronomical Society of the Pacific*, 113, 764
- Gray, R. O., Corbally, C. J., & Burgasser, A. J. 2009, *Stellar spectral classification*, Vol. 15 (Princeton university press)
- Hachisu, I., & Kato, M. 2001, *The Astrophysical Journal*, 558, 323
- Han, X. L., Zhang, L.-Y., Shi, J.-R., et al. 2018, *Research in Astronomy and Astrophysics*, 18, 068
- Hellier, C. 2001, *Publications of the Astronomical Society of the Pacific*, 113, 469
- Hou, W., Luo, A.-l., Li, Y.-B., & Qin, L. 2020, *The Astronomical Journal*, 159, 43
- Jiang, B., Luo, A., Zhao, Y., & Wei, P. 2013, *Monthly Notices of the Royal Astronomical Society*, 430, 986
- King, A. R., & Cannizzo, J. K. 1998, *The Astrophysical Journal*, 499, 348
- Knigge, C., Long, K. S., Hoard, D., Szkody, P., & Dhillon, V. 2000, *The Astrophysical Journal Letters*, 539, L49
- La Dous, C. 1994, *Space science reviews*, 67, 1
- McInnes, L., Healy, J., & Melville, J. 2018, arXiv preprint arXiv:1802.03426
- Morales-Rueda, L., & Marsh, T. 2002, *Monthly Notices of the Royal Astronomical Society*, 332, 814
- Ritter, H., & Kolb, U. 2003, *Astronomy & Astrophysics*, 404, 301
- Rodríguez-Gil, P., Shahbaz, T., Marsh, T. R., et al. 2015, *Monthly Notices of the Royal Astronomical Society*, 452, 146, doi: [10.1093/mnras/stv1244](https://doi.org/10.1093/mnras/stv1244)
- Rodríguez-Gil, P., Shahbaz, T., Torres, M. A. P., et al. 2020, *Monthly Notices of the Royal Astronomical Society*, 494, 425, doi: [10.1093/mnras/staa612](https://doi.org/10.1093/mnras/staa612)
- Roulston, B. R., Green, P. G., & Kesseli, A. Y. 2020, arXiv preprint arXiv:2006.01199
- Shao, J. 1993, *Journal of the American statistical Association*, 88, 486
- Szkody, P. 1987, *The Astrophysical Journal Supplement Series*, 63, 685
- Szkody, P., Anderson, S. F., Brooks, K., et al. 2011, *The Astronomical Journal*, 142, 181
- Szkody, P., Diczynski, B., Ho, A. Y., et al. 2020, *The Astronomical Journal*, 159, 198
- Warner, B. 2003, *Cataclysmic variable stars*, Vol. 28 (Cambridge University Press)
- Zhang, Y.-Y., Deng, L.-C., Liu, C., et al. 2013, *The Astronomical Journal*, 146, 34
- Zhao, G., Zhao, Y.-H., Chu, Y.-Q., Jing, Y.-P., & Deng, L.-C. 2012, *Research in Astronomy and Astrophysics*, 12, 723
- Zorotovic, M., Schreiber, M. R., Parsons, S. G., et al. 2016, *Monthly Notices of the Royal Astronomical Society*, 457, 3867

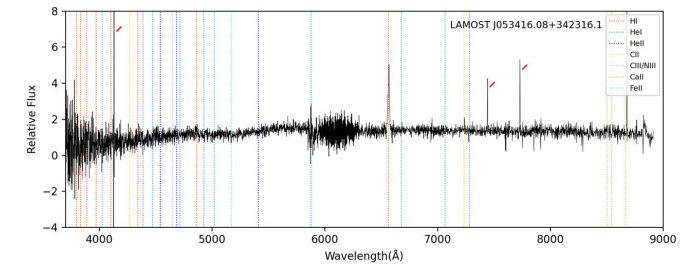
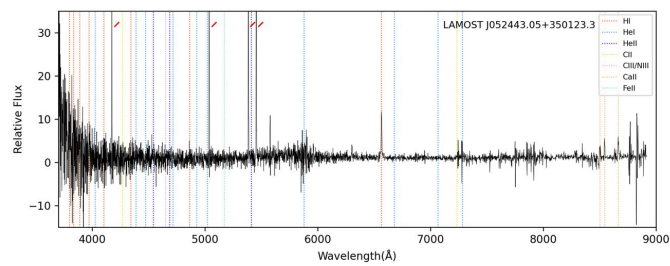
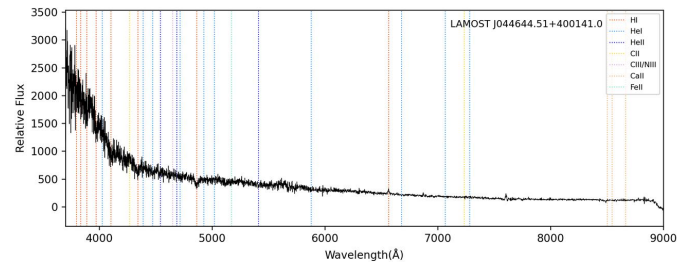
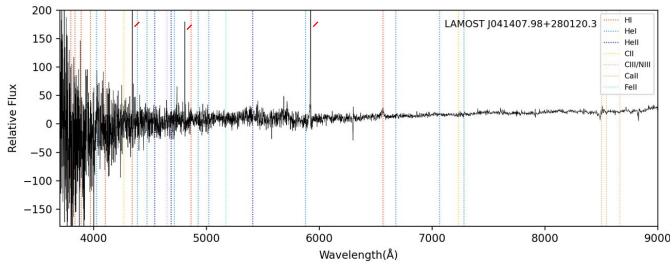
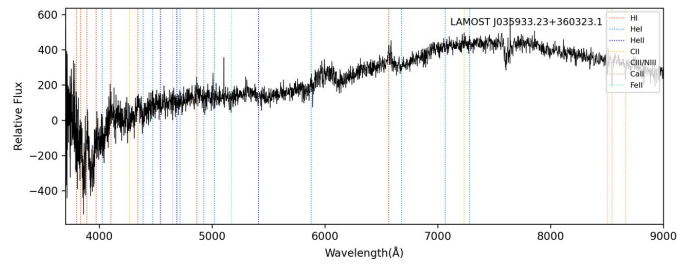
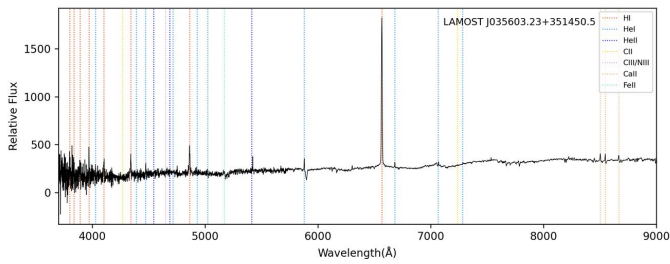
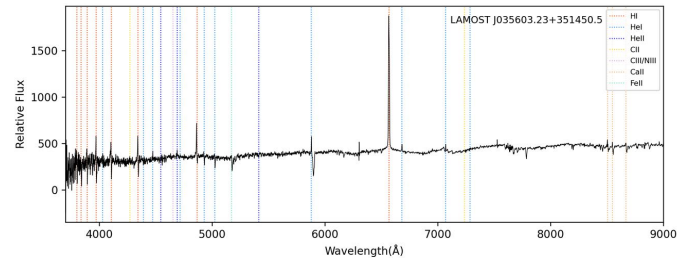
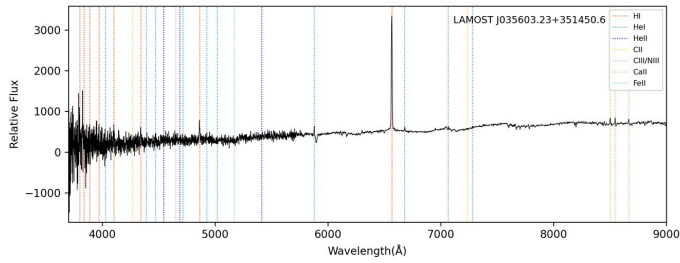
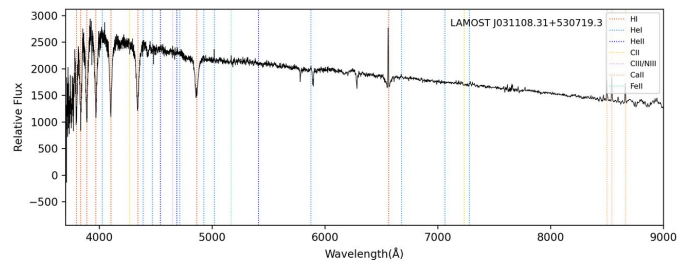
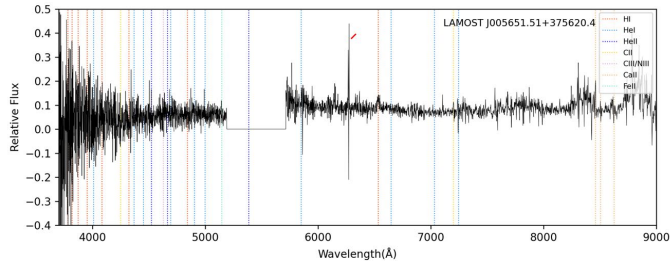
APPENDIX  
THE LAMOST SPECTRA

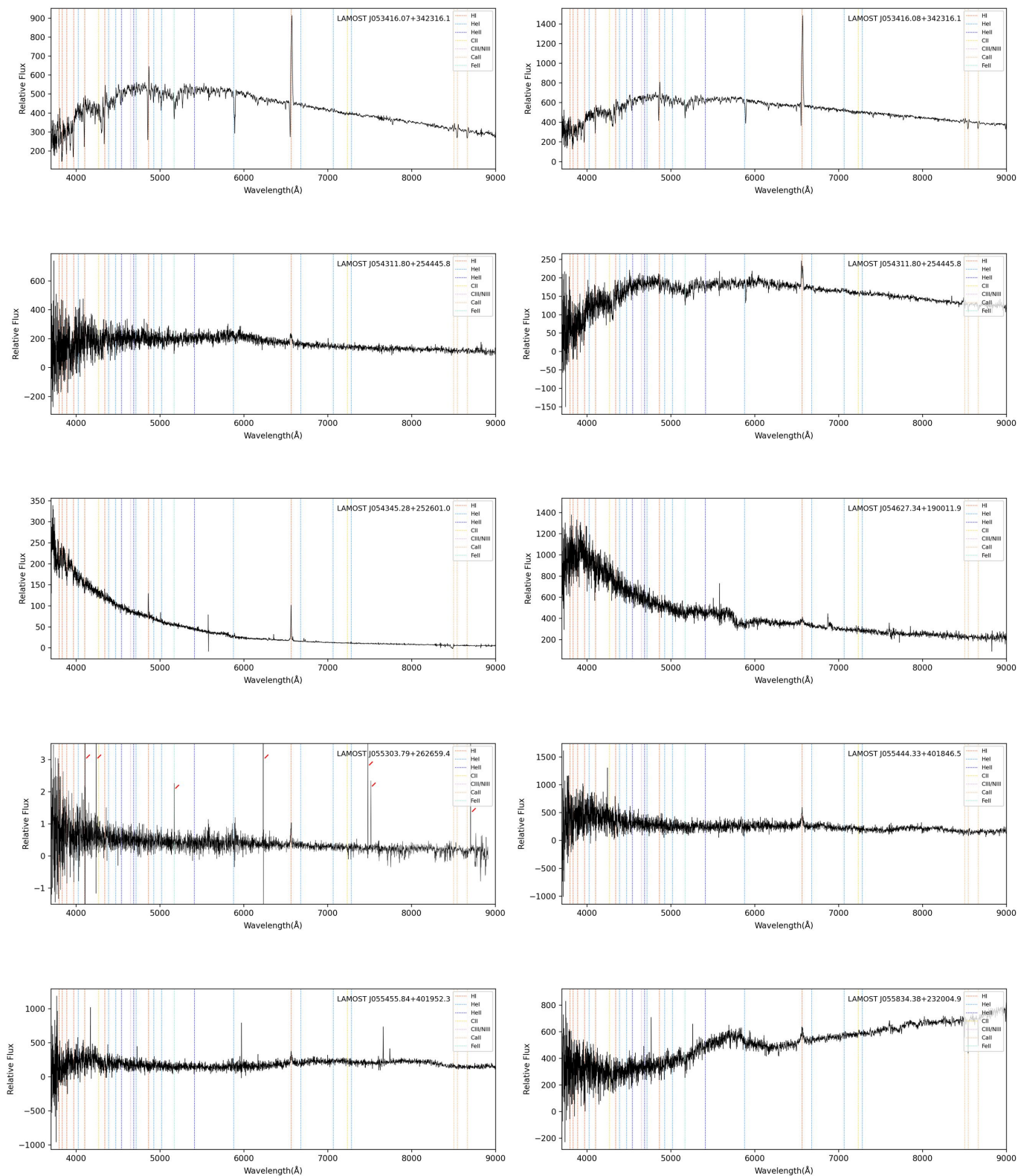


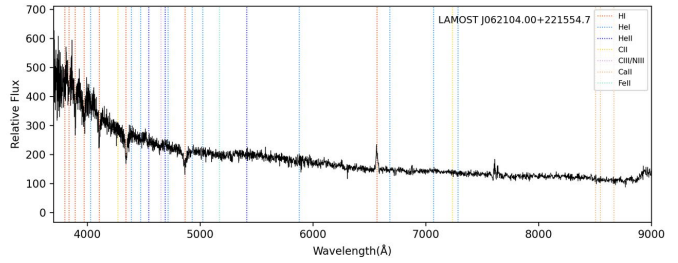
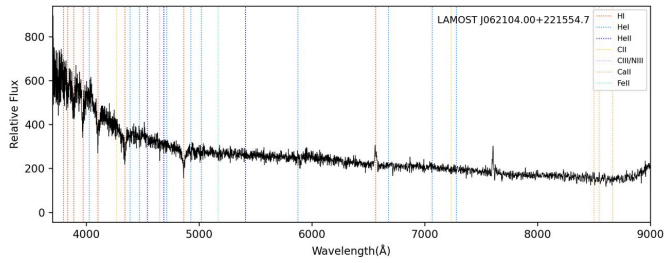
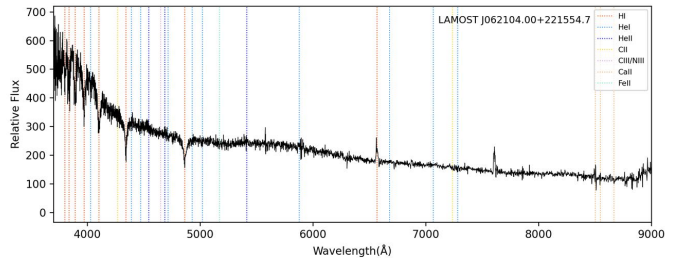
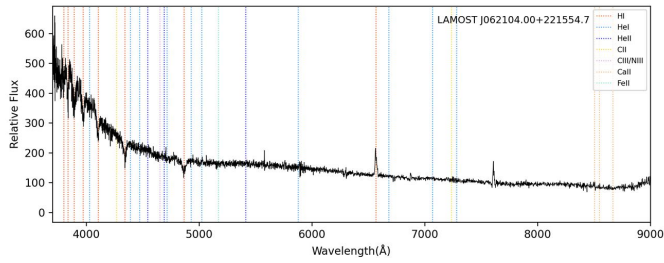
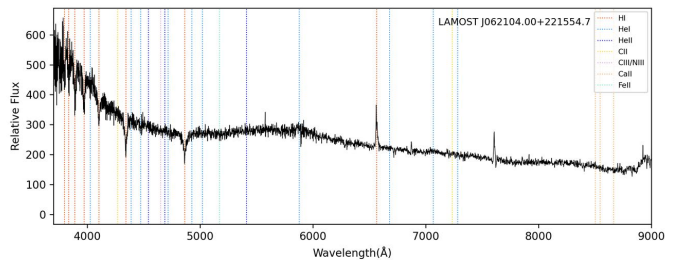
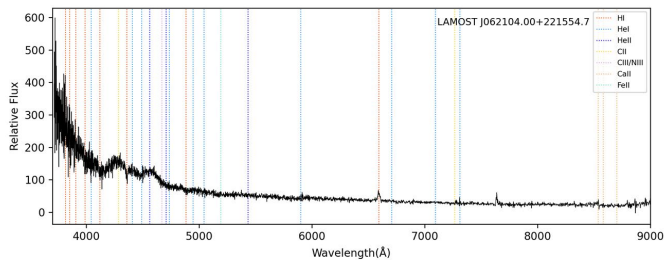
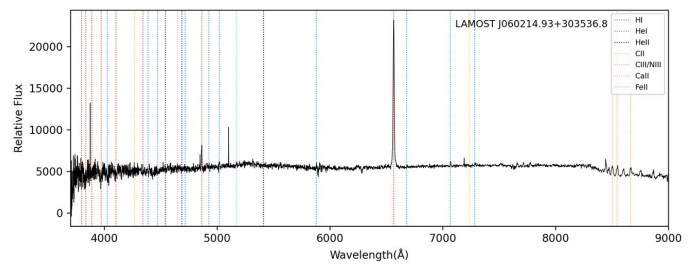
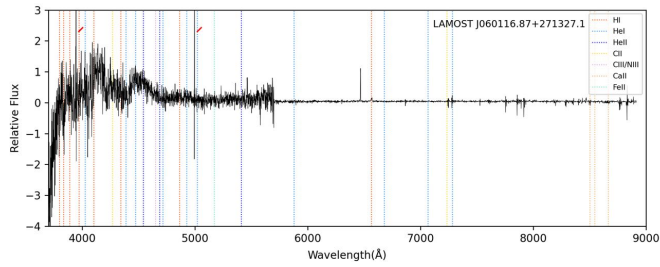
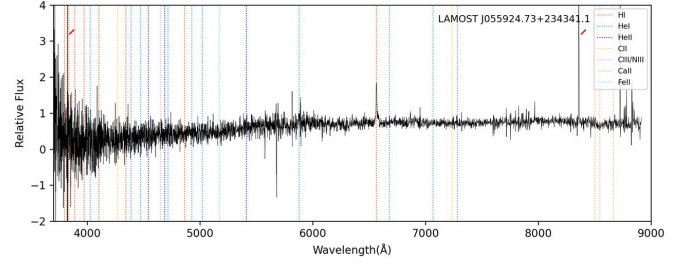
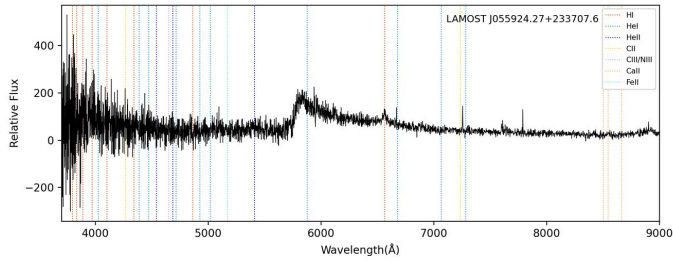




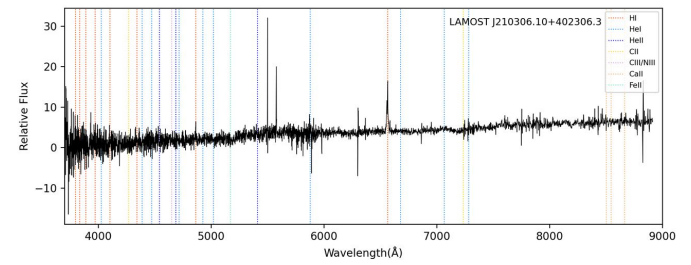
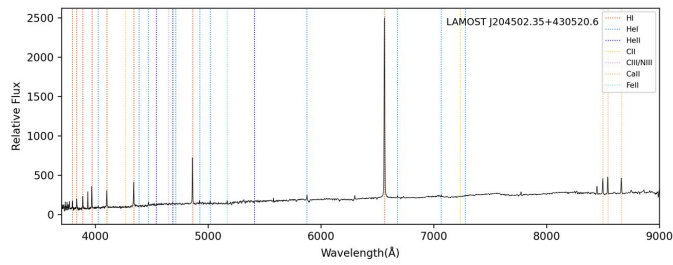
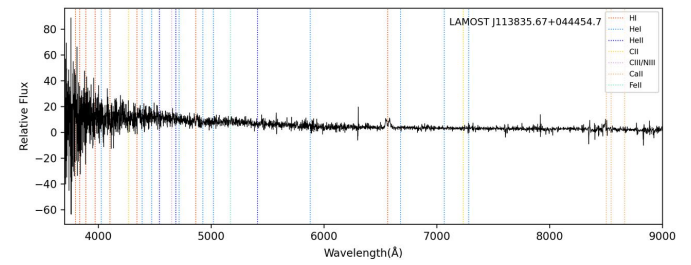
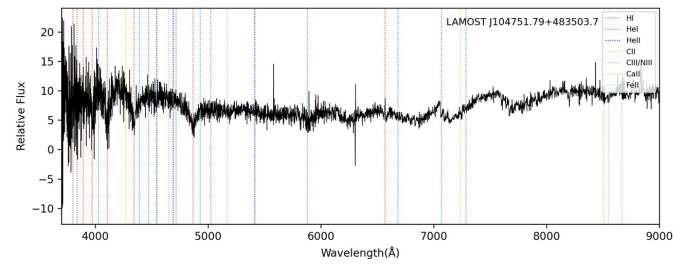
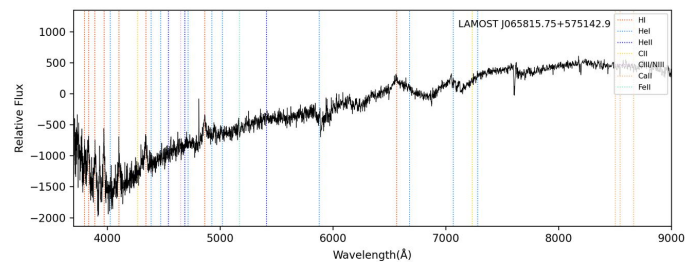
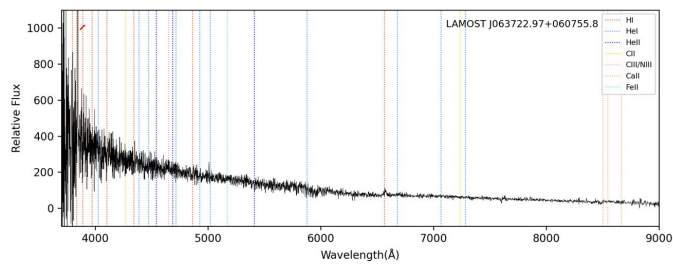
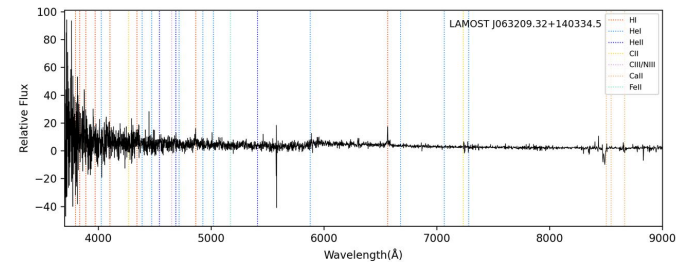
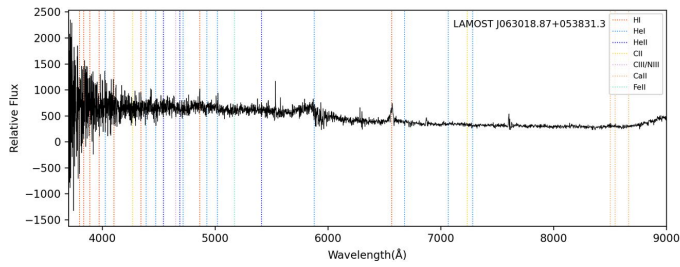
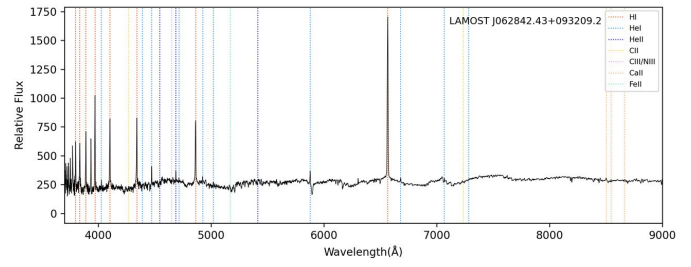
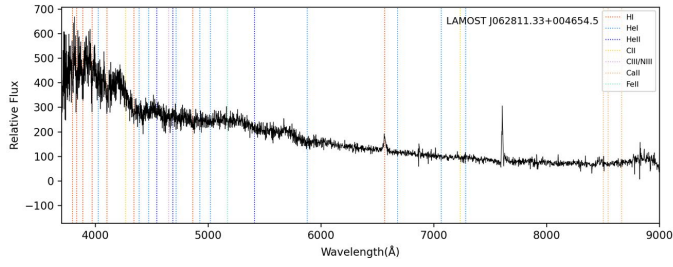
**Figure 10.** 21 spectra of 20 new confirmed CV candidates in LAMOST DR6 (ordered by increasing RA). The wavelength range is from 3700 Å to 9000 Å. Cosmic ray hits are marked by short red slashes.

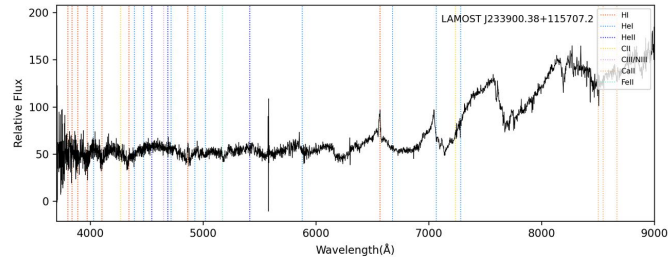












**Figure 11.** 52 spectra of 32 new possible CV candidates in LAMOST DR6 (ordered by increasing RA). The wavelength range is from 3700 Å to 9000 Å. Cosmic ray hits are marked by short red slashes.